ELSEVIER

Int. J. Therm. Sci. 41 (2002) 664–672

International Journal of Thermal Sciences

www.elsevier.com/locate/ijts

Heat transfer and rivulet structures formation in a falling thin liquid film locally heated ☆

Oleg A. Kabov [a,b,*], Benoit Scheid [b], Irina A. Sharina [a], Jean-Claude Legros [b]

[a] *Institute of Thermophysics SB RAS, 630090, Novosibirsk, Russia*

[b] *Microgravity Research Center, Chimie-Physique EP, Université Libre de Bruxelles C.P. 165/62, Avenue F.D. Roosevelt, 50, B-1050, Bruxelles, Belgium*

Received 20 October 2001; accepted 8 February 2002

Abstract

An experimental investigation of the heat transfer from a local heat source to a liquid film falling down a vertical plate is performed. The thermocapillary counterflow, induced by non-uniform heating, causes a deformation of the film surface having a horizontal bump-shape. This shape becomes unstable above a critical value of the imposed heat flux and deforms into vertical downstream rivulets. This variation of patterns is expected to modify significantly the heat transfer through the film. Experiments are carried out at atmospheric pressure with three varying parameters: the streamwise heater length, the Reynolds number and the imposed heat flux density. Velocimetry, shadowgraphy and infrared thermography are used to study the behavior of the interface and the heat transfer. We put in evidence the presence of a thermocapillary counter flow producing a stagnation line at the upper edges of the horseshoe structures, beyond the instability threshold, and observe a decrease of the heat transfer with the Reynolds number.

Keywords: Liquid film; Thermocapillarity; Rivulet structures; Heat transfer

1. Introduction

Thin liquid films are widely spread in different branches of industry. For instance, they are used in low-pressure evaporators for concentrating nutritional liquids, rectification columns, sea water desalinators, etc. In order to reduce the thermal resistance of falling liquid films, substrates are often built with complicated shapes. Among enhanced surfaces, one can find a so-called "fluted tube", a vertically oriented tube with longitudinal fins, used in sugar refinery for heating and concentrating processes.

The main features of films flowing along such enhanced surfaces are: small Reynolds number flow regimes, non-uniformity of the heating and strong deformation of the liquid-gas interface [1]. Furthermore, the mean surface tension tends to thin the film at the top of the grooves. Small Reynolds number flows also take place at final stage of film evaporating devices and in the region of residual layer in wavy film motion [2]. The liquid film is usually provided from sprayers, being subcooled up to the saturation temperature. The resulting Marangoni effect, caused by the non-uniformity of the surface tension at the liquid-gas interface, can also strongly influence the flow dynamics and thus the heat transfer.

Results of purposely-oriented investigations of heat transfer and crisis phenomena in flowing liquid films under non-uniform heating were reported in [3–8]. Local heaters with different sizes were used. Film flow of perfluortriethylamine and of ethyl alcohol solution over a vertical plate with a local heater of 6.5×13 mm^2 size was studied in [3–5]. The phenomenon of "regular horseshoe-like structures formation" was identified. A liquid bump is formed in the region of the upper edge of the heating element. Beyond a critical heat flux, rivulets aligned with the flow start from this bump and distribute spanwise with a fixed wavelength. An important thinning of the film takes place between them. Experimental and theoretical data about the influence of control parameters on the heat transfer, the rivulet structure formation and the film breakdown are quite limited [3–9].

The aim of the present work is to investigate the features of the heat transfer with a local heat source and to deter-

☆ This article is a follow-up a communication presented by the authors at the ExHFT-5 (5th World Conference on Experimental Heat Transfer, Fluid Mechanics and Thermodynamics), held in Thessaloniki in September 24–28, 2001.

* Correspondence and reprints
E-mail address: okabov@ulb.ac.be (O.A. Kabov).

1290-0729/02/$ – see front matter
PII: S1290-0729(02)01361-3

Nomenclature

A	Constant in the Eq. (3)	$W{\cdot}m^{-2}{\cdot}K^{-n}$
A_{noz}	nozzle width	m
B	heater width	m
c	thermal capacity of liquid	$J{\cdot}kg^{-1}{\cdot}K^{-1}$
C	concentration of ethyl-alcohol by mass in the mixture	%
d_m	distance between thermocouples centers	m
g	gravitational acceleration	$m{\cdot}s^{-2}$
G	mass flow rate	$kg{\cdot}s^{-1}$
h_0	initial film thickness	m
l_ν	scale of viscosity-gravitational interaction, $=(\nu^2/g)^{1/3}$	m
L	streamwise heater length	m
L_b	length of the thermal developed region	m
n	The exponent in the Eq. (3)	
Nu_{h0}	Nusselt number $=\alpha_0 \cdot h_0/\lambda_0$	
Pr_0	Prandtl number	
q	local heat flux	$W{\cdot}cm^{-2}$
q_v	heat flux determined according to the power release	$W{\cdot}cm^{-2}$
Q	power released from the heater	W
q_{vrol}	heat flux corresponding to the structures formation	$W{\cdot}cm^{-2}$
Re	Reynolds number	
T_0	initial temperature of flowing liquid film	°C
T_F	the bulk temperature of the liquid film	°C
T_W	wall temperature	°C
ΔT_{hc}	temperature drop across the stainless steel plate, measured by thermocouples	K
ΔT_0	temperature difference between the wall and the one of the initial film $=T_W-T_0$	K
U_{sur}	velocity on the surface of the liquid film	$m{\cdot}s^{-1}$
x, y	Cartesian coordinates	m
X	distance from the upper edge of the heater to the thermocouple	m

Greek symbols

α_0	heat transfer coefficient	$W{\cdot}m^{-2}{\cdot}K^{-1}$
Λ	wavelength of the regular structures	m
λ	liquid thermal conductivity	$W{\cdot}m^{-1}{\cdot}K^{-1}$
λ_{mm}	thermal conductivity of stainless steel	$W{\cdot}m^{-1}{\cdot}K^{-1}$
μ	liquid dynamic viscosity	$kg{\cdot}m^{-1}{\cdot}s^{-1}$
ν	liquid kinematics viscosity	$m^2{\cdot}s^{-1}$

Subscripts

0	properties of the liquid calculated at T_0
L, R	left or right part of the heater
SUR	parameter for the surface of the liquid film

mine the dynamics of the surface flow in presence of rivulet structures. The experiment was controlled by three parameters. They are, with their respective values, the streamwise heater length (2.22 mm, 4.02 mm), the Reynolds number (0.06–9) and the heat flux density (0–9 $W{\cdot}cm^{-2}$). The span of the heaters was, by an order of magnitude, greater than the rivulet structure wavelength in order to avoid edge effect.

2. Experimental setup

2.1. Experimental apparatus

The experiments are carried out at atmospheric pressure and the measurements are performed in stationary conditions. Fig. 1 shows a picture and a sketch of the experimental set-up including the test section, the optical set-up, the heat power supply, the flow meter and the density sensor. A thermostatic bath (not shown on the picture) closes the circulating loop of the liquid and keeps the liquid at constant temperature T_0. Humidity and temperature of the surrounding atmospheric air are kept constant with $50 \pm 5\%$ and $20 \pm 0.5\,°C$, respectively. The liquid is pumped from the thermostatic bath into the film sprinkler fixed at the top of the main plate (substrate). It consists of a buffer chamber, a multi-hole distributor and a nozzle with a calibrated 250 μm flat slot.

The main plate is made in textolite of size $250 \times 334 \times 46\ mm^3$ in width, length and deep respectively, and is kept at constant temperature by an internal system of 8 mm diameter channels through which the liquid is also pumped. The falling film is of 191.6 mm wide and is collected by a vessel at the end of the substrate. Three heaters of different sizes are embedded into the main plate at certain distances from the nozzle. They are located on one hand in the fully developed region of the film flow, but in the other hand in the area of the waveless liquid-gas interface [2,10].

The cross section of the heaters are shown in Figs. 2(a) and 3(a). In the present research, two heaters of sizes $4.02 \times 68.1\ mm^2$, named H2 (second position from the nozzle), and $2.22 \times 68.05\ mm^2$, named H3 (third position from the nozzle) are used. Results of the experiments using the first heater of sizes $6.75 \times 109\ mm^2$ are presented in [6].

Two pairs of thermocouples are embedded at both sides of each stainless steel plate as depicted in Figs. 2(b) and 3(b). They allowed determination of the heat flux by measuring the temperature difference ΔT_{hc} across the heating element. The cavity around the heaters was filled with a mixture of epoxy resin and charcoal. A 2.5 mm thick layer of the same mixture also covered the surface around the heaters of sizes

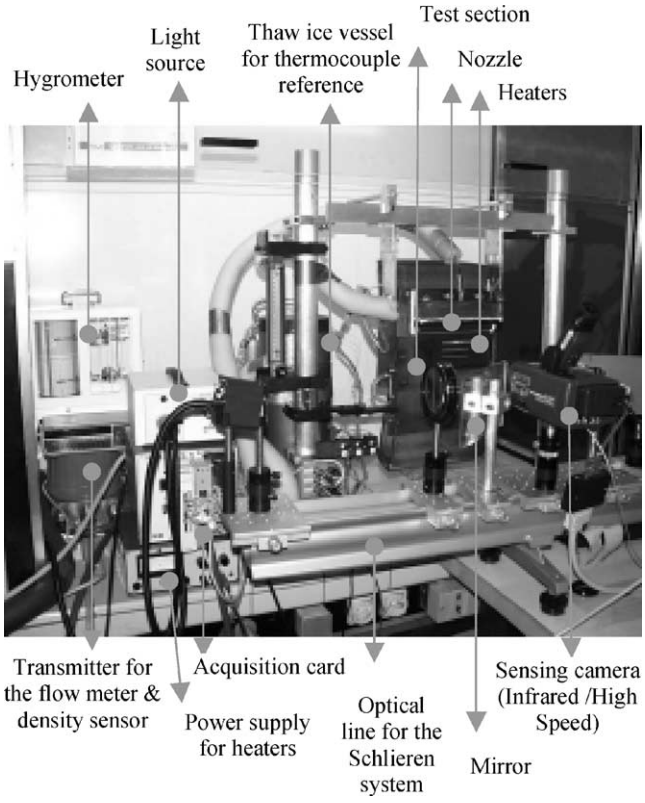

Fig. 1. Experimental set-up, (a) photo, (b) sketch (sizes in mm).

85 × 200 mm. The thermal conductivity of the mixture is by a factor 100 less than the one of the stainless steel in order to reduce the heat losses. The whole test section is carefully polished.

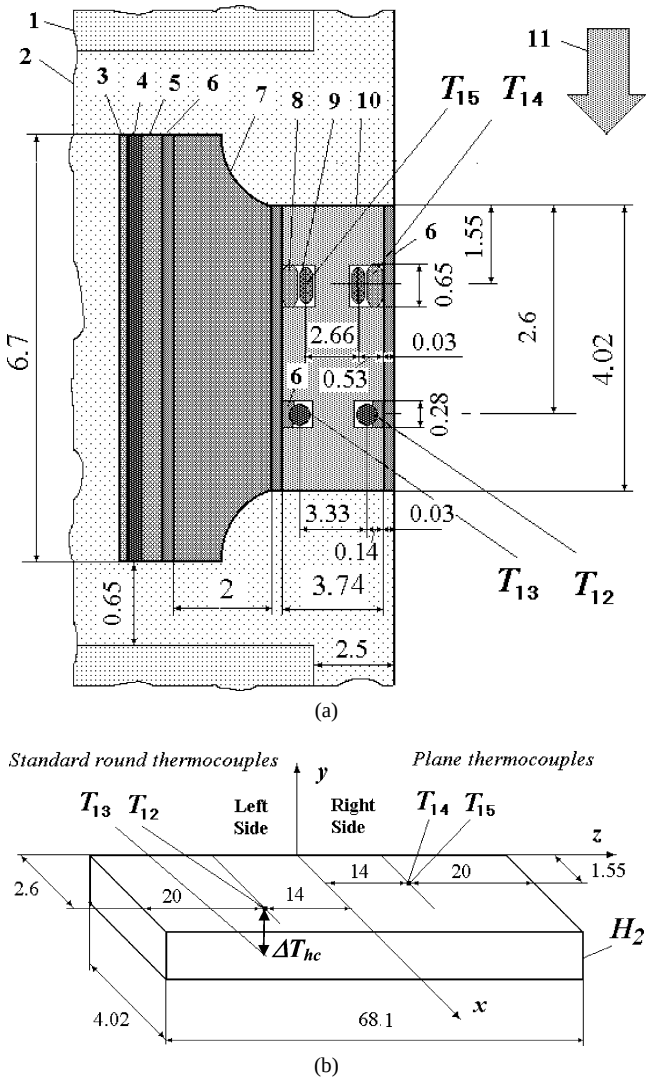

Fig. 2. (a) Design of the heating element H2. 1—textolite, 2—heat-insulating mixture, 3—electrical insulation, 4—heat source, 5—ceramic plate, 6—tin, 7—copper block, 8—copper cover, 9—thermocouples, 10—stainless steel plate, 11—flow direction (sizes in mm). (b) Arrangement of thermocouples on the stainless steel plate of the heating element H2 (see 10 in Fig. 2(a)).

2.2. Method of measurements

The temperature at the heater surface is calculated by taking into account the depth at which the thermocouples are embedded. Additional thermocouples were used to measure the initial temperature of the film T_0, and the one of the ambient air. The heat flux is determined locally using the temperature difference over the thickness of the stainless steel plate ΔT_{hc}, according to the formula

$$q_{\mathrm{L,R}} = \Delta T_{hc\mathrm{L,R}} \cdot \lambda_{mm}/d_m$$

where the subscripts L and R indicate the left and the right parts of the heater. The uncertainty on $q_{\mathrm{L,R}}$ is 6% at working regimes. Besides, the global heat flux is determined

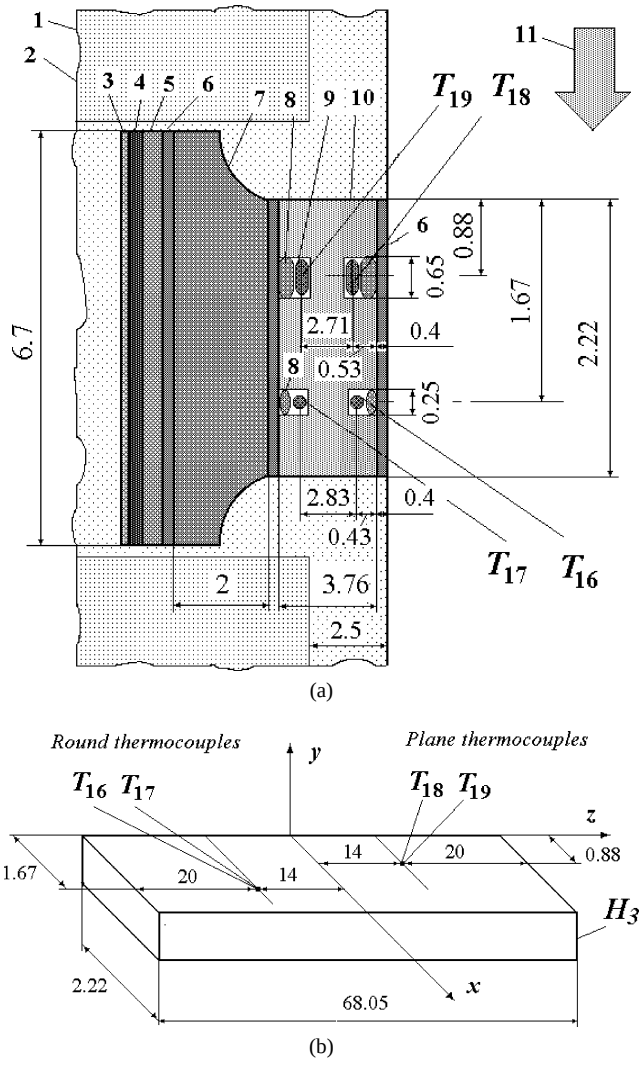

Fig. 3. (a) Design of the heating element H3 (see denomination in Fig. 2(a)). (b) Arrangement of thermocouples on the stainless steel plate of the heating element H3 (sizes in mm).

by knowing the power released to the heating element, according to

$$q_v = Q/(LB).$$

Solution of 25% ethyl alcohol in water is used as working liquid. The initial liquid temperature is $T_0 = 20\,^{\circ}\mathrm{C}$, chosen equal to the ambient temperature. A micro Motion's ELITE CMF010 sensor offers accurate mass flow and density measurements. The absolute error of the device does not exceed 0.01%. The knowledge of the fluid properties is based on its concentration. Its value is obtained from a polynomial dependence on the fluid density [11]. The initial film thickness is calculated from the Nusselt dependence

$$h_0 = l_\nu (3\,Re)^{1/3}$$

with

$$l_\nu = (\nu^2/g)^{1/3} \quad \text{and} \quad Re = \frac{G}{A_{\mathrm{noz}}\mu}$$

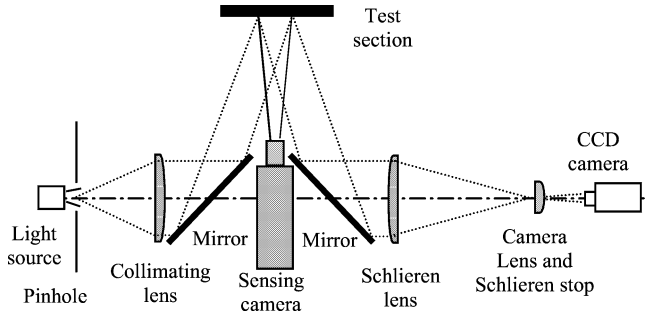

Fig. 4. Schematic top view of the optical set-up combining a Schlieren system and a sensing camera (infrared or high-speed camera).

The data acquisition is performed by a National Instrument device with a frequency of 416 Hz broadcast between 24 channels (thermocouples, heating power, density sensor and flow meter). The effective acquisition rate for each channel is 1–5 Hz depending on the number of samples used for the average (4–17 samples). The data acquisition is controlled through a LabVIEW interface.

The sensing camera placed in front of the test section is either a high-speed camera for the velocity field measurement or an infrared camera for the temperature field measurement, both at the interface. A Schlieren optical system is mounted in line, parallel to the test section. Two mirrors are used with the appropriate orientation to not invade the field of view of the sensing camera. A top view sketch is shown on Fig. 4. The purpose of the Schlieren system here is to visualize qualitatively the deformations of the liquid-gas interface.

3. Experimental results

3.1. Surface velocity measurement

A high-speed camera is used to measure the velocity at the interface by tracking particles. Aluminum particles with an average size of 5 μm are used as tracers. They are blown at the liquid-gas interface where they agglomerate to give higher reflectivity. Fig. 5 shows a good agreement between results of the tests performed in isothermal conditions and the so-called Nusselt theory from which the surface velocity can be calculated as

$$U_{\mathrm{sur}} = g h_0^2/2\nu.$$

The deviation of measurement from theory is less than 1% for $Re \leqslant 1$. Therefore, we can assume that the tracers stay in one layer at the interface and do not perturbed the flow. Each velocity given in Fig. 5 is the average of values measured along the heater span by intervals of 10 mm. This spanwise distribution of the velocity is reported in Fig. 6. The abscissa $z = 0$ corresponds to the left side of the test section. The liquid film is at 43 mm from this left side. The vertical solid lines on Fig. 6 indicate the position of heater edges while the dotted lines indicate the location of the thermocouples

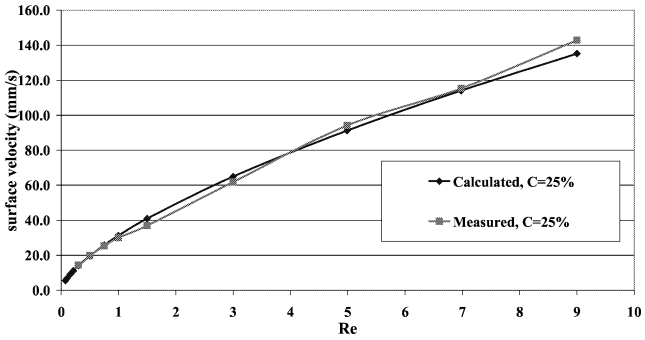

Fig. 5. Velocity at the interface, U_{sur} (see text), of the liquid film in isothermal conditions.

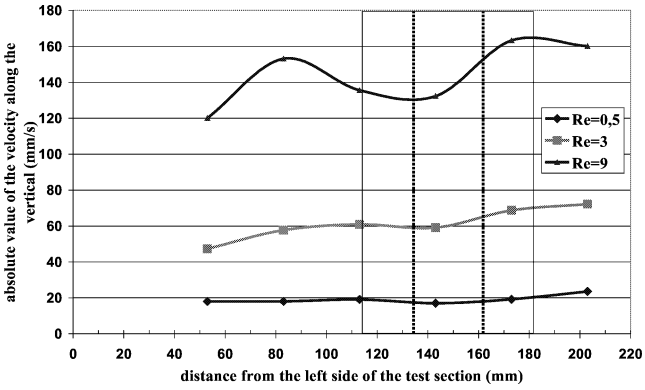

Fig. 6. Distribution of the surface velocity along the spanwise direction.

inside the heating element. Fig. 6 shows the uniformity of the velocity along the z-axis where the deviation is less than 15% for $Re = 0.5$ and $Re = 3$, while it raises up to 25% for $Re = 9$.

Fig. 7 shows rivulet structure instability obtained for a heat flux density above the threshold one, q_{vrol}. The image is obtained by optical Schlieren technique, where a deformed zone is seen as dark and a flat one as bright. The critical heat flux is found to increase with the Reynolds number as obtained in previous results [5] where it was found experimentally that $q_{vrol} \propto Re^{1.09}$. We also obtain in the present work that the critical heat flux decreases with increasing the streamwise heater length.

Fig. 8 presents three thermograms of the film surface, one at instability onset (Fig. 8(a)), and the others beyond it (Fig. 8(b)). The streamwise and spanwise temperature distribution over the film surface is essentially non-uniform. The maximal temperature is observed between rivulets, where the liquid film is thinner.

Fig. 9 presents a sequence of corresponding pictures showing the tracking of particles. Particles are not visible in the heater zone but dashed lines represent their trajectories. Time starts from the first image. The horseshoe structures are made visible by the aluminum particles blown at the interface above and below the heating zone. The tracers indicate that the two-dimensional flow is broken and a strongly nonlinear three-dimensional flow takes place. The particles flow down following the streamline of the rivulet. However, some of them, localized just at the top of the

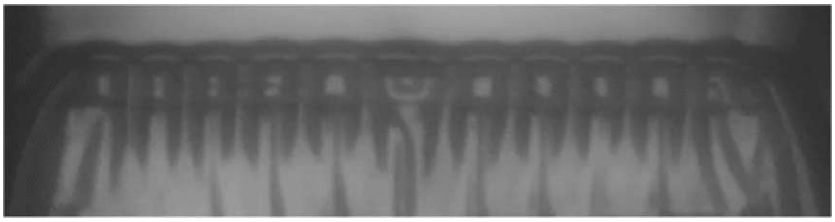

Fig. 7. Rivulet structures (H2, 25% ethyl-alcohol solution).

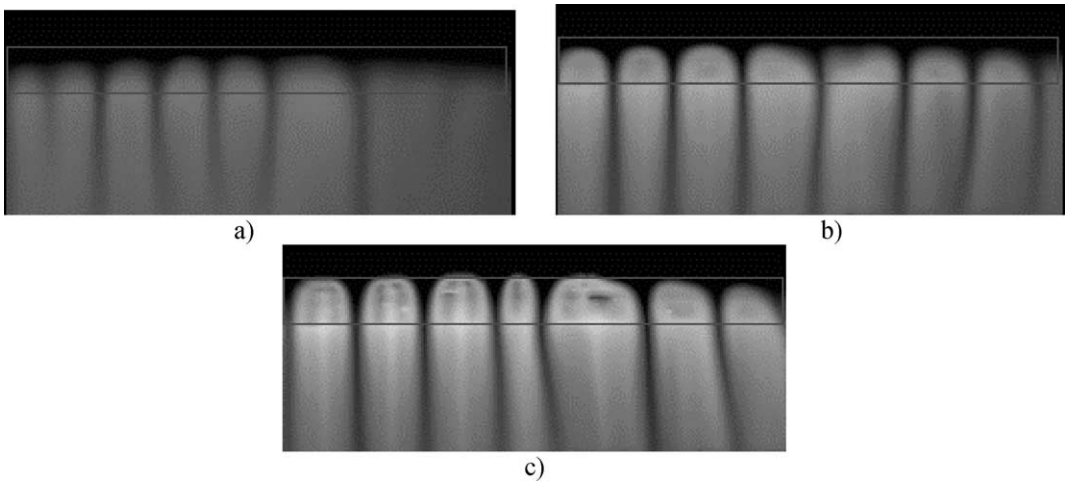

Fig. 8. Temperature field at the surface of the film, $Re = 1$, H2. (a) $q = 4.7$ W·cm^{-2} at onset of the instability, (b) $q = 5.5$ W·cm^{-2}, (c) $q = 5.8$ W·cm^{-2}.

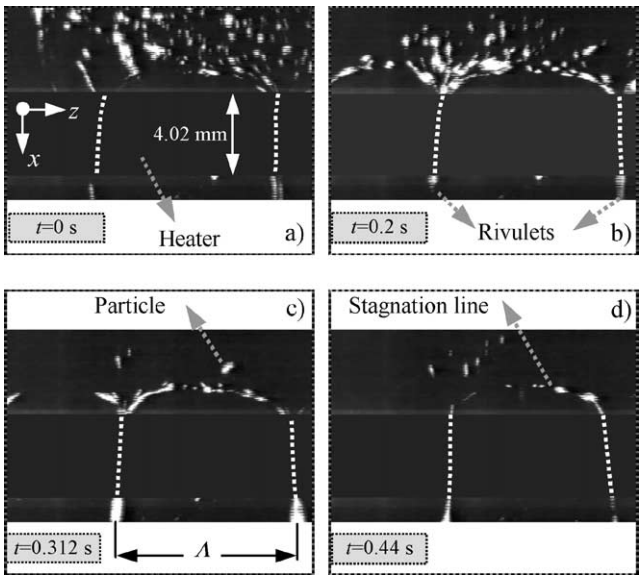

Fig. 9. Sequence of particle tracking, evidencing the stagnation point, for $Re = 0.5$, H2, and recorded at a rate of 125 frame·s^{-1}. The time, referenced from the first picture, is indicated at the bottom-left corner of each picture.

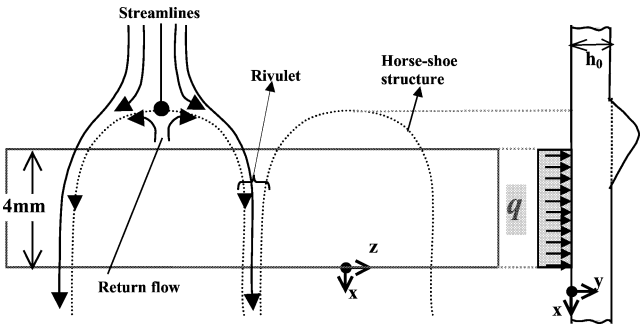

Fig. 10. Schematic model (front and side view) of the flow in the presence of instability.

horseshoe structure stay almost immobile during time. These facts provide the evidence of a stagnation point as predicted by the two-dimensional theoretical analysis [6,8,9]. The tracers, after being stopped at the stagnation point, move slowly along the z-axis until to reach a rivulet streamline. A return flow between rivulets was also observed. The maximum distance between the upstream edge of the heater and the stagnation point is 1.1–1.5 mm. Fig. 10 shows the model of the streamlines based on the above observations.

3.2. Local heat flux distribution

In order to check the reliability of the whole experimental setup, some specific tests are performed and sources of error identified. The heat losses into the main plate and the local heat flux distribution can be evaluated by the ratios q_L/q_v and q_R/q_v, respectively for the left and the right parts of the heaters. Fig. 11 shows the value of these ratios for the heater H2 at two different regimes. The divergence between the local heat flux at the right and left parts of the heater does not exceed 3% for $Re = 9$ and 6% for $Re = 6$. Given that q_L and q_R are measured at different x-coordinates (see Figs. 2(b) and 3(b)), we can maintain that the heater construction satisfies the condition $q = \text{const}$ within the range of experimental errors. The same verification can be done for the heat loss by noting that the values of $q_{L,R}/q_v$ for different runs are close to the unity and the maximum deviation observed is 7% for the smallest value of q_v ($q_v \geqslant 0.8$ W·cm^{-2}).

Fig. 12 shows the influence of the Reynolds number on the local heat fluxes for the heater H2 and at fixed $q_v = 1$ W·cm^{-2}. The same conclusions than previously, about the uniformity of the heat flux and the heat losses into the substrate, can be drawn for $Re \geqslant 1.5$. Nevertheless, for $Re < 1.5$, the right local heat fluxes can be up to 30% larger than the left one. At the same time the heat losses become prominent (more than 50% for the left part) and special care must be taken in interpretation of the results for such small

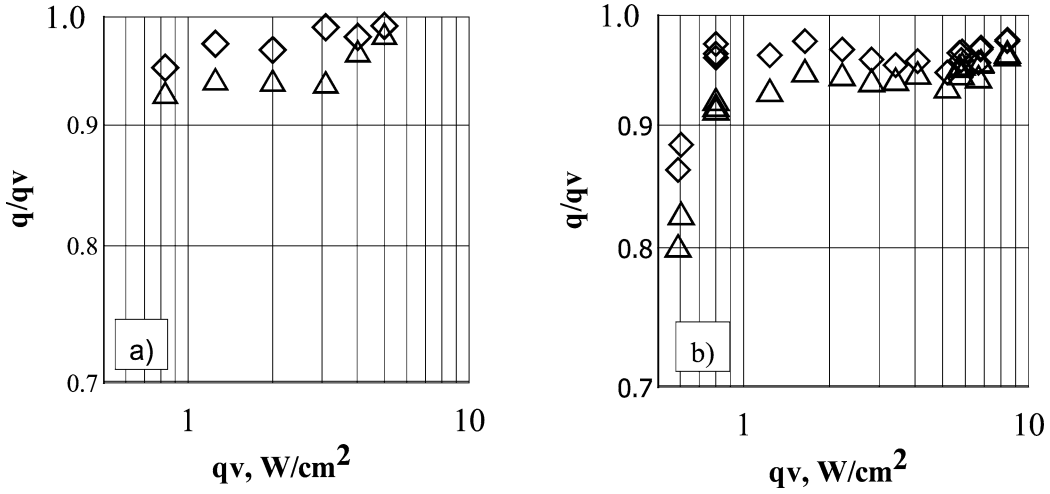

Fig. 11. Local heat fluxes at the right (triangle) and the left (diamond) parts of heater H2. (a) $Re = 6$; (b) $Re = 9$.

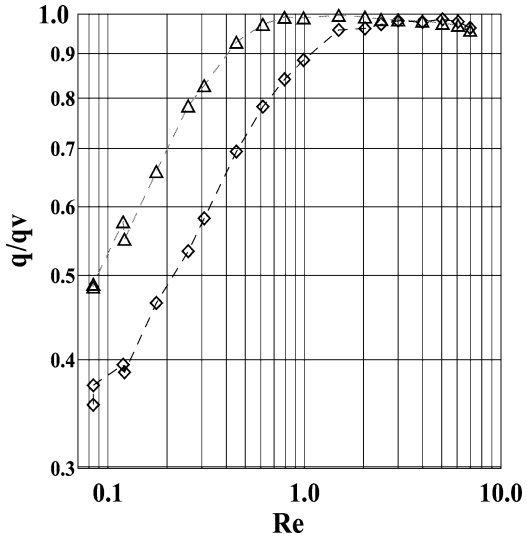

Fig. 12. Dependence of the relative heat flux density versus the Reynolds number at the right (triangle) and the left (diamond) parts of heater H2, $q_v = 1\ \mathrm{W{\cdot}cm^{-2}}$.

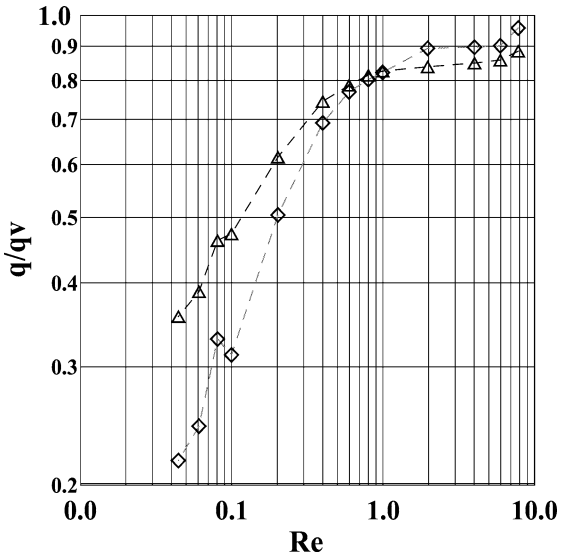

Fig. 13. Same as Fig. 11 for H3 and $q_v = 1\ \mathrm{W{\cdot}cm^{-2}}$.

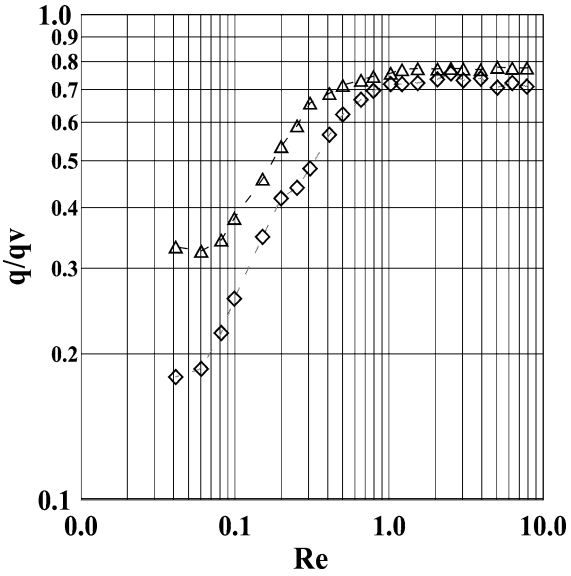

Fig. 14. Same as Fig. 11 for H3 and $q_v = 3\ \mathrm{W{\cdot}cm^{-2}}$.

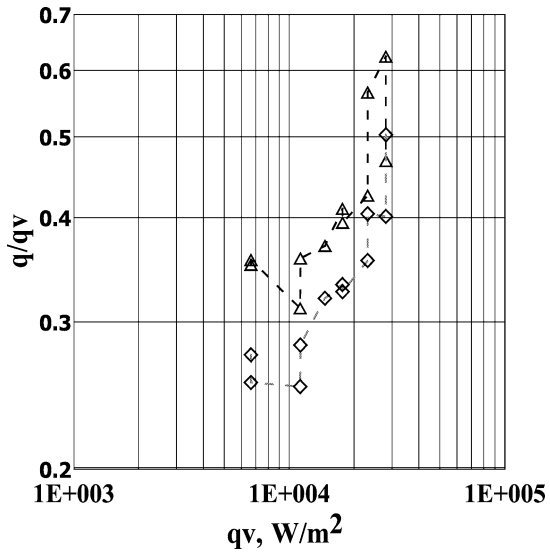

Fig. 15. Dependences between the average and the local heat fluxes at the right (triangle) and the left (diamond) parts of heater H2, $Re = 0{,}06$.

flow rate. Figs. 13 and 14 show similar data for the heater H3 at two different values of $q_v = 1$–$3\ \mathrm{W{\cdot}cm^{-2}}$. The difference between local heat flux at the right and left parts of the heater does not exceed 8% at $q_v = 1\ \mathrm{W{\cdot}cm^{-2}}$ for $Re \geqslant 0.4$ as well as at $q_v = 3\ \mathrm{W{\cdot}cm^{-2}}$ for $Re \geqslant 0.6$.

The deviations increase again drastically for smaller value of *Re*. Therefore, the uniformity of the heating ($q =$ const) for both heaters (H2 & H3) appears to be satisfied, in terms of experimental accuracy, for *Re* numbers higher than a certain limit. Moreover, this limit increases with the average heat flux q_v. Besides, the deviation of the local heat fluxes $q_{\mathrm{L,R}}$ from the average one, q_v, is much higher for heater H3 than for heater H2. This fact can be assigned to the influence of the streamwise length of the heater, which is twice smaller for H3 than for H2. Nevertheless, for extremely small Reynolds number, this strong dependence between $q_{\mathrm{L,R}}$ and q_v is also observed for H2 as depicted in Fig. 15 for $Re = 0.06$. This seems physically reasonable since the heat losses into the substrate itself become maximum for minimum flow rate.

We observe also from the results presented in Figs. 12–15 that the local heat flux is systematically higher at the right part than at the left part of the heater. However, the fact that this effect is more pronounced only for small *Re* confirms the presence of a redistribution of heat fluxes and temperatures within the heating element for sufficiently small *Re*.

This redistribution is due to the change of the weighted-mean temperature of the liquid with the mass along the heater, and the dependence of the local heat transfer coefficient on the x-coordinate. It results in a relative equalization

of the wall temperature. Therefore, the heat flux as a function of the x-coordinate monotonically decreases, and this validates qualitatively the existing numerical calculations [12].

3.3. Heat transfer at the thermal developing region

Here, the regime is adjusted in such a way that the heater to be located in the thermal developing region [13]. Fig. 16 shows, for heater H2, the dependence on the heat flux of the temperature difference between the wall and the one of the initial film $\Delta T_0 = T_W - T_0$. The results are compared with the following semi-empirical dependence obtained by Gimbutis [13], for the wall condition $q = \text{const}$,

$$Nu_{h0} = 2.06\left[1 + 0.0443\left(Pr_0 \cdot Re_0 \cdot \frac{h_0}{X}\right)^{4/3}\right]^{1/4} \quad (1)$$

As shown by Gimbutis, Eq. (1) satisfactorily describes some available experimental data on convection in laminar and laminar-wave regimes of the flow. In Eq. (1) all the properties of the liquid are calculated at the temperature T_0.

The length of the heat boundary layer can be determined from the dependence [13]

$$L_b = 0.139 \cdot l_v \cdot Pr_0 \cdot Re^{4/3}$$

and is equal to $L_b = 5.55$ mm for $Re = 9$ and $C = 25\%$. The experimental data for the left part of the heater deviate from Eq. (1) by 4.2% at $\Delta T_0 = 1.5$ K and 5.5% at $\Delta T_0 = 8.8$ K. The local heat transfer coefficient is systematically higher at the right part than at the left part of the heater. The exponential interpolation is 16.9% higher for the right part and according to Eq. (1), this deviation is a function of the parameter $(X_L/X_R)^{1/3}$ and should be 18.8%. Therefore, Eq. (1) satisfactorily predicts the dependence of the distance from the upper edge of the heater. Furthermore, the Nusselt number

$$Nu_{h0} = \alpha_0 \cdot h_0/\lambda_0, \quad \text{with } \alpha_0 = q_{L,R}/\Delta T_0 \quad (2)$$

remains constant and the exponent n in the following dependence

$$q = A(\Delta T_0)^n \quad (3)$$

is close to 1 (A is a constant). All these facts are in accordance with previous experimental data [2–4,13].

3.4. Heat transfer at small Reynolds numbers

In Fig. 17 are presented data on heat transfer at the left part of the heater H2, for different values of the Reynolds number. The comparison with Eq. (1) is drawn for $Re = 0.06$ and $Re = 9$. According to Eq. (1) in the case of heat transfer at the stabilized section, when $L_b < X$ ($Re \leqslant 2$), the Nusselt number should be constant and should be equal to 2.06. Experimental data show strong dependence of the heat transfer coefficient on the heat flux density. The exponent n in Eq. (3) is also depicted in Fig. 17. It is ranged between 0.67 and 1.46. In Fig. 17, the experimental curves for $Re \geqslant 2$ are close to the line calculated from Eq. (1) for $Re = 9$. Data for $Re < 2$ are located below this line and the heat transfer coefficient decreases by a factor 30 between $Re = 9$ and $Re = 0.06$.

On the contrary, Eq. (1) predicts an increase of the heat transfer coefficient with a decrease of the Reynolds number. This opposite trend can be explained partly by the fact that Eq. (1) is valid when the temperature difference at the measurement point is based on the mixed bulk temperature of the film rather than on ΔT_0. The data obtained by infrared thermography indicate a large difference between T_0 and the bulk temperature of the film, which increases with decreasing the flow rate. According to our estimations based

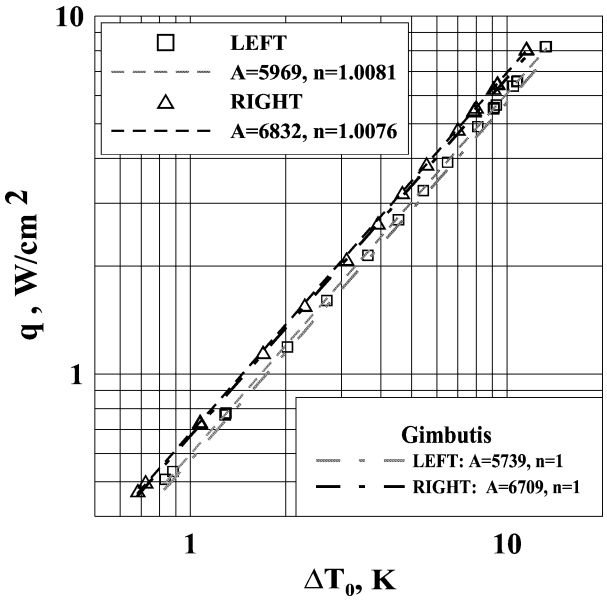

Fig. 16. Heat flux versus temperature difference at the right (triangle) and the left (diamond) parts of heater H2, $Re = 9$.

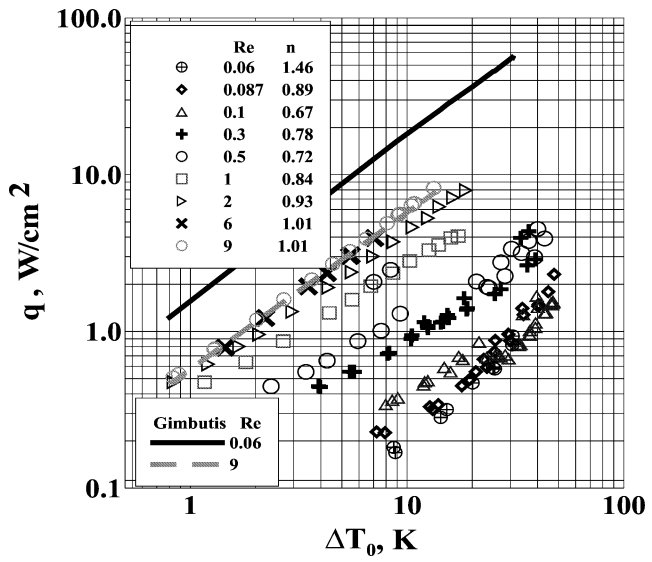

Fig. 17. Heat transfer at the left part of the heater H2.

on this effect, the intensity of the heat transfer coefficient decreases by a factor from 3 to 5. So, it seems that the drop in the heat transfer coefficient cannot be explained completely by the difference between T_0 and the bulk temperature of the film. Because the density of heat flux at the wall and at the interface is an unknown nonlinear functions of x-coordinate, due to convection and evaporation, it is impossible to calculate the bulk temperature of the film.

As noticed in the paragraph 3.2 the uncertainty for local heat flux density increases sensitively as Re decreases (see Figs. 11–14). The data for $Re < 1$ are presented in Fig. 17 to show qualitatively the dependence of heat transfer coefficient (Eq. (2)) versus *Re* number.

At the same time, the important decrease of heat transfer intensity appears when strong deformations are observed at the interface and it seems then to be directly related to the Marangoni effect. The decrease of the heat transfer coefficient with the Reynolds number were observed also in [3]. The exponent n in the Eq. (3) is ranged between 0.69 and 1.0 when *Re* number varies from 0.68 to 9. For 25% ethyl alcohol solution in water flowing over a vertical plate with a local heater of $6.5 \times 13\ \text{mm}^2$ size at $T_0 = 30\ ^\circ\text{C}$ and $\Delta T_0 = 8$ K, the heat transfer coefficient decreases by a factor 4.8. Further investigations are needed to elucidate this mechanism.

4. Conclusions

(1) The heater construction satisfied the condition $q =$ const, in terms of experimental accuracy, for $Re \geqslant 1.5$. The heat losses were negligible, within the range of experimental errors, for $Re \geqslant 1.5$ and sufficiently long heater ($L \geqslant 4$ mm). Nevertheless, special care must be taken in interpretation of the results for small flow rate, because of the presence of a redistribution of heat fluxes in the heating element.

(2) The horseshoe structures were made visible by the aluminum tracers blown at the interface, which indicated that the two-dimensional flow is broken in the vicinity of the heating element and a strongly non-linear three-dimensional flow takes place. The existing of a stagnation line at the top of the horseshoe structure as predicted by the two-dimensional theoretical analysis was confirmed. A return flow between two rivulets was also observed.

(3) Semi-empirical dependence derived in [13] satisfactorily described the heat transfer at the thermal developing region.

(4) The important decrease of the heat transfer coefficient with the Reynolds number was observed. Further investigations are needed to elucidate this effect.

Acknowledgements

The authors gratefully acknowledge the support of this work by the Commission of the European Communities under grant ERB IC15-CT98-0908, by financial support from the Belgian Office for Scientific (OSTC) and the Interuniversity Poles of Attraction Program IV-06, Belgium State, Federal Office for Scientific, Technical and Cultural Affairs.

References

[1] L. Zhao, R.L. Cerro, Experimental characterization of viscous film flows over complex surfaces, Internat. J. Multiphase Flow 18 (4) (1992) 495–516.

[2] S.V. Alekseenko, V.E. Nakoryakov, B.G. Pokusaev, Wave Flow of Liquid Films, Begell House, New York, 1994.

[3] O.A. Kabov, A.V. Diatlov, I.V. Marchuk, Heat transfer from a vertical heat source to falling liquid film, in: G.P. Celata, R.K. Shah (Eds.), Proc. First Internat. Symp. on Two-Phase Flow Modeling and Experimentation (Rome, Italy), Vol. 1, 1995, pp. 203–210.

[4] O.A. Kabov, E.A. Chinnov, Heat transfer from a local heat source to a subcooled falling liquid film evaporating in a vapor-gas medium, Russian J. Engrg. Thermophys. 7 (1–2) (1997) 1–34.

[5] O.A. Kabov, Formation of regular structures in a falling liquid film upon local heating, Thermophys. Aeromech. 5 (1) (1998) 547–551.

[6] O.A. Kabov, I.V. Marchuk, A.V. Muzykantov, J.-C. Legros, E. Istasse, J.L. Dewandel, Regular structures in locally heated falling liquid films, in: Proc. 2nd Int. Symp. on Two-Phase Flow Modelling and Experimentation (Pisa, Italy), Vol. 2, 1999, pp. 1225–1233.

[7] B. Scheid, O.A. Kabov, C. Minetti, P. Colinet, J.-C. Legros, Measurement of free surface deformation by reflectance-schlieren technique, in: E.W.P. Hahne, W. Heidemann, K. Spindler (Eds.), Proc. 3rd European Themal Sciences Conference (Heidelberg, Germany), Edizioni ETS, Pisa, Italy, Vol. 1, 2000, pp. 651–657.

[8] O.A. Kabov, J.-C. Legros, I.V. Marchuk, B. Scheid, Deformation of the free surface in a moving locally-heated thin liquid layer, Fluid Dynamics 36 (3) (2001) 521–528.

[9] I.V. Marchuk, O.A. Kabov, Numerical modelling of thermocapillary reverse flow in thin liquid films under local heating, Russian J. Engrg. Thermophys. 8 (1–4) (1998) 17–46.

[10] P.L. Kapiza, Wave flow of thin layer of viscous fluid, Zhurn. Eksper. Teor. Fiz. 18 (1) (1948) 3–28.

[11] V.N. Stabnikov, T.M. Roiter, T.V. Protsyuk, Ethyl alcohol, Pishchevaya promyshlennost, Moscow, 1976.

[12] I.V. Marchuk, O.A. Kabov, Numerical simulation of heat transfer in a falling liquid film with allowance for heat conduction in heaters, Russian J. Engrg. Thermophys. 10 (2) (2000) 147–165.

[13] I. Gimbutis, Heat Transfer to a Falling Fluid Film, Mokslas, Vilnius, 1988.